Title

High-throughput radio-TLC analysis

Authors

Wang, Jia

Rios, Alejandra

Lisova, Ksenia

et al.

Publication Date

2020-03-01

DOI

10.1016/j.nucmedbio.2019.12.003

Peer reviewed

HHS Public Access

Author manuscript

Nucl Med Biol. Author manuscript; available in PMC 2021 March 01.

Published in final edited form as:

Nucl Med Biol. 2020 ; 82-83: 41–48. doi:10.1016/j.nucmedbio.2019.12.003.

High-throughput radio-TLC analysis

Jia Wang[1,2,#], **Alejandra Rios**[1,3,#], **Ksenia Lisova**[1,3], **Roger Slavik**[4,5], **Arion F. Chatziioannou**[1,3,4], **R. Michael van Dam**[1,2,3,4,*]

[1]Crump Institute for Molecular Imaging, University of California Los Angeles, Los Angeles, CA, 90095, USA

[2]Department of Bioengineering, University of California Los Angeles, Los Angeles, CA, 90095, USA

[3]Physics in Biology and Medicine Interdepartmental Graduate Program, University of California Los Angeles, Los Angeles, CA, 90095, USA

[4]Department of Molecular & Medical Pharmacology, David Geffen School of Medicine, University of California Los Angeles, Los Angeles, CA, 90095, USA

[5]Ahmanson Translational Imaging Division, University of California Los Angeles, Los Angeles, CA, 90095, USA

Abstract

Introduction—Radio thin layer chromatography (radio-TLC) is commonly used to analyze purity of radiopharmaceuticals or to determine the reaction conversion when optimizing radiosynthesis processes. In applications where there are few radioactive species, radio-TLC is preferred over radio-high-performance liquid chromatography due to its simplicity and relatively quick analysis time. However, with current radio-TLC methods, it remains cumbersome to analyze a large number of samples during reaction optimization. In a couple of studies, Cerenkov luminescence imaging (CLI) has been used for reading radio-TLC plates spotted with a variety of isotopes. We show that this approach can be extended to develop a high-throughput approach for radio-TLC analysis of many samples.

Methods—The high-throughput radio-TLC analysis was carried out by performing parallel development of multiple radioactive samples spotted on a single TLC plate, followed by simultaneous readout of the separated samples using Cerenkov imaging. Using custom-written

[*]Corresponding author: mvandam@mednet.ucla.edu; Tel: +1(310) 206-6507; Address: California Nanosystems Institute, room 4323, 570 Westwood plaza, Los Angeles, CA90095-7227.

[7]Author Contributions

J.W. and A.R performed experiments and analyzed data. K.L. assisted with experiments involving [18F]FET and R.S. assisted with experiments involving [177Lu]Lu-PSMA-617. J.W., A.R., A.F.C., and R.M.V. contributed to the experimental design. J.W., A.R., and R.M.V. wrote the manuscript. R.M.V. supervised the project. All authors have provided feedback on the manuscript and approved the final version.

[#]Contributed equally to this work

[8]Disclosures

The authors have no conflicts of interest to declare.

MATLAB software, images were processed and regions of interest (ROIs) were drawn to enclose the radioactive regions/spots. For each sample, the proportion of integrated signal in each ROI was computed. Various crude samples of [^{18}F]fallypride, [^{18}F]FET and [^{177}Lu]Lu-PSMA-617 were prepared for demonstration of this new method.

Results—Benefiting from a parallel developing process and high resolution of CLI-based readout, total analysis time for eight [^{18}F]fallypride samples was 7.5 min (2.5 min for parallel developing, 5 min for parallel readout), which was significantly shorter than the 48 min needed using conventional approaches (24 min for sequential developing, 24 min for sequential readout on a radio-TLC scanner). The greater separation resolution of CLI enabled the discovery of a low-abundance side product from a crude [^{18}F]FET sample that was not discernable using the radio-TLC scanner. Using the CLI-based readout method, we also observed that high labeling efficiency (99%) of [^{177}Lu]Lu-PSMA-617 can be achieved in just 10 min, rather than the typical 30 min timeframe used.

Conclusions—Cerenkov imaging in combination with parallel developing of multiple samples on a single TLC plate proved to be a practical method for rapid, high-throughput radio-TLC analysis.

Keywords

Radiopharmaceutical analysis; Radiosynthesis optimization; Quality control testing; Radiochemical purity; Thin-layer chromatography; High-throughput analysis

2 Introduction

Thin layer chromatography (TLC) is a technique used to separate the chemical components of a mixture to identify its composition. TLC has multiple uses ranging from analysis of purity and yield in chemical synthesis[2,3], separation of species in biological assays[4], and, in conjunction with a radiation detector, analysis of radiopharmaceuticals used for positron emission tomography (PET)[5–7], single-photon emission computed tomography (SPECT)[8,9], or targeted radiotherapy[10,11]. In particular, radio-TLC is useful as a means to measure the conversion of radionuclide incorporation into the target radioactive product during synthesis development and optimization; its use is further extend as a quality control (QC) testing of the final formulated radiopharmaceutical to ensure radiochemical purity and radiochemical identity[12] before administering to patients. Radio-high-performance liquid chromatography (radio-HPLC) is another chromatography technique for analysis, and is particularly useful when distinct separation of multiple compounds is needed. However, in many radiopharmaceutical analysis applications, radio-TLC is sufficient and is preferred over radio-HPLC due to its simplicity, quantitative measurement of [^{18}F]fluoride amount (can be underestimated in HPLC due to retention on the column[13]), relatively short measurement time[14], and low need for maintenance.

Typically, a TLC plate (spotted with a small amount of the sample and then developed with a mobile phase) will be analyzed using a radio-TLC scanner, in which a radiation detector is moved along the plate to obtain measurements of emitted radiation as a function of distance along the plate. Most radio-TLC scanners (e.g. AR-2000, Eckert & Ziegler) use gas-based

radiation detectors that are sensitive to gamma radiation as well as beta particles. Downsides of such systems are the requirements for continuous supply of gas as well as periodic calibrations. Other radio-TLC scanners (e.g. miniGITA, Raytest) are based on crystal scintillators and photodiodes that do not require a gas supply. Sometimes, different detectors can be installed depending on the radionuclides of interest. Spatial resolution is related to the range of the type(s) of radiation of interest. High resolution can be achieved by employing detectors sensitive and specific to short-ranged particles (e.g. alpha, beta). For longer-ranged radiation (e.g. gamma rays), resolution is much lower, but can be somewhat improved if a collimator is installed (at the expense of sensitivity).

Typically, the TLC plates used are 60 – 100 mm long and take 10 – 30 min to develop. The length of the TLC plate is needed both to achieve adequate chemical separation and provide enough readout resolution. The scanning time depends on activity level, but typically 1–3 min is sufficient to analyze each TLC lane[15,16].

Our laboratory is developing high-throughput radiolabeling methods for optimization of synthesis conditions or preparation of compound libraries, resulting in the need to perform significant numbers of TLC separations and analyze the resulting TLC plates, requiring significant time for development and scanning.

Though some scanners, e.g. AR-2000, have space to install multiple TLC plates which can be scanned automatically in sequence, the overall analysis time is additive and still remains long[17]. To reduce the readout time, we have looked into alternative approaches for readout of TLC plates. Other than scanning detectors, several techniques have been used to more efficiently read radio-TLC plates. One such technique is electronic autoradiography. Such systems, e.g. Instant Imager (Canberra Packard) have a large-area multiwire proportional counter detector, on which multiple radio-TLC plates can be imaged simultaneously. This system has been shown to be accurate and suitable for imaging of a wide range of isotopes (Tc-99m, I-124, F-18, Cu-64, C-11)[15,18–20]. Radio-TLC plates have also been imaged in a more cumbersome two-step process by first exposing a phosphor screen that is subsequently scanned with a phosphor imaging system[21] (e.g. Perkin Elmer Cyclone Plus). Additional types of detectors have been used for simultaneous readout at multiple positions along a TLC plate thus avoiding the need for scanning. For example, using a 64×1 array of scintillator crystals above a photodiode array, Jeon *et al.* quantified samples spotted at multiple locations with different radioisotopes (Tc-99m, F-18) and found excellent agreement with an AR-2000 scanner [16]. In another example, Maneuski *et al.* used a pixelated solid-state Timepix silicon detector to obtain a 2D image of a partial radio-TLC plate spotted with an unspecified ^{18}F-containing compound [22]; however the detector size is small and multiple expensive detectors would be needed to image a full radio-TLC plate or multiple plates.

A more scalable approach is Cerenkov luminescence imaging (CLI) in which radiation is detected indirectly via Cerenkov light emission, and the overall detection area can be scaled with a suitable optical system rather than larger detector. In this CLI approach, Cerenkov light is emitted by radiation particles that have sufficient energy to exceed the speed of light

in the medium through which they are traveling (i.e. the TLC plate matrix itself, or a transparent material placed over the TLC plate).

CLI-based detection of compounds containing a wide variety of radionuclides has been demonstrated, including H-3, C-11, C-14, F-18, P-32, Cu-64, Ga-68, I-124, and I-131. Originally reported as a method to observe radioactivity in microfluidic chips [23,24], CLI is also used for *in vivo* optical imaging [25,26], intraoperative imaging [27,28], and has been reported for readout of radio-TLC plates [29]. A significant advantage of CLI is that, if the thickness of the transparent medium is comparable to the radiation particle range, the spatial resolution is limited by the particle range. For example, for positrons from F-18, the spatial resolution when using poly-dimethylsiloxane (a transparent polymer with similar index of refraction to glass) was shown to be hundreds of microns [23]. (Even though the positrons will eventually lead to the production of 511 keV gamma rays, there is negligible production of Cerenkov light due to gamma rays passing through the thin transparent layer. In contrast, due to the long range of gamma rays, scanners based on gamma detection, even with the smallest available collimators, have spatial resolution of at least many millimeters. Another attractive feature of this technique is that it can be used for imaging of β^- particles (mostly involved in therapeutic applications in cancer), which do not emit gamma rays (as occurs after positron emission) and thus are not easily imaged by systems based on gamma detection [25].

Park *et al.* reported a proof-of-concept demonstration in 2011, showing the possibility to use a commercial small-animal luminescence imaging system (IVIS 200, Caliper Life Sciences) to perform CLI of a developed radio-TLC plate spotted with an unspecific mixture of ^{131}I-containing compounds[29]. The quantified percentage of luminescence in each of four ROIs compared favorably to the analysis using a conventional radio-TLC scanner (AR-2000). Furthermore, the CLI approach augmented the resolution between separated species, while imaging could be performed rapidly (1 min). Using a custom-built optical imaging system, Spinelli *et al.* later showed that the imaging time of radio-TLC plates with spotted samples of [^{68}Ga]Ga-DOTANOC (7 kBq) could be reduced (compared to CLI) by placing the plates in contact with a phosphor-containing intensifying screen [30]. Recently, Ha *et al.* investigated the effect of different types of TLC plates (differing backing materials, stationary phase type and thickness, and addition of fluorescent indicator) by placing multiple spots of various radioisotope solutions (e.g. H-3, P-32, I-124, and I-131) on TLC plates, imaging these plates directly and quantifying relative intensity between spotting locations[31], showing the possibility to significantly increase the CLI signal and sensitivity. An interesting feature of this work was a demonstration that multiple radio-TLC plates (16) could be positioned within the large field of view of the small animal scanner (IVIS Spectrum or IVIS Lumina II, Caliper) for simultaneous imaging, and thus speeding the readout when multiple plates are analyzed. However, the high cost (an order of magnitude higher than a conventional radio-TLC scanner) and large size of the small animal scanners may not be practical for many radiochemistry laboratories.

Though demonstrating the potential for high-throughput readout of radio-TLC plates, Ha *et al.* did not develop the TLC plates (i.e. did not perform sample separations). It can be assumed that this step would be very time-consuming and cumbersome for a large number

of TLC plates, and that this time and effort would dominate the overall radio-TLC analysis process.

In this paper, we tackle this missing step and we show a practical approach for the complete analysis of radio-TLC plates (both separation and readout) in a high-throughput, time- and labor-efficient manner. This was accomplished by leveraging the high resolution of CLI and optimizing the sample volume to enable multiple samples to be spotted close together on the same TLC plate. All samples could then be rapidly developed in parallel (leveraging the high imaging resolution to enable very short separation distances) and then read out simultaneously using a compact Cerenkov imaging system [32]. We demonstrate high-throughput radio-TLC analysis of complex mixtures of ^{18}F-labeled and ^{177}Lu-labeled radiopharmaceuticals including (S)-N-((1-Allyl-2-pyrrrolidinyl)methyl)-5-(3-[^{18}F]fluoropropyl)-2,3-dimethoxybenzamide ([^{18}F]fallypride), [^{18}F]fluoroethyl-tyrosine ([^{18}F]FET) and [^{177}Lu]Lu-PSMA-617 for assessment of radiochemical purity or reaction conversion. Interestingly, the Cerenkov imaging readout clearly showed small peaks that were not discernable with a conventional radio-TLC scanner (miniGITA), was able to identify anomalies in the spotting/separation process that also would not be apparent when using a conventional scanner and resulted in superior accuracy and precision compared with conventional radio-TLC scanning.

3 Experimental Section

3.1 Preparation and developing of radio-TLC plates

Samples of crude radiopharmaceuticals were deposited with a micropipettor 15 mm from the edge of the TLC plate. Deposited volume was 1.0 μL unless otherwise specified. Typically, 4 samples were spotted on each 50 mm × 60 mm TLC plate along the 50 mm edge at 1 cm spacing so that 4 “lanes” would be formed during development. We also performed spotting of 8 samples at 0.5 cm spacing on 50 mm × 35 mm TLC plates. For mock TLC plates, we spotted with [^{18}F]fluoride/[^{18}O]H_2O at multiple points on the TLC plate and then immediately dried the plate (i.e. no development was performed).

[^{18}F]Fallypride samples (synthesized according to Figure S1) were deposited onto silica gel 60 F_{254} sheets (aluminum backing) and developed with 60% MeCN in 25 mM NH_4HCO_2 with 1% TEA (v/v). The solvent front took ~8 min to travel 55 mm (i.e. 35 mm separation distance), or ~2.5 min to travel 30 mm (i.e. 15 mm separation distance).

Samples of [^{18}F]FET and the fluorinated intermediate (see Figure S1) were spotted onto silica gel 60 F_{254} sheets (aluminum backing) and developed with a 80:20 (v/v) mixture of MeCN and DI water. The solvent front took ~9 min to travel 55 mm (i.e. 35 mm separation distance). In some cases, single samples were spotted onto longer TLC plates (Baker-flex silica gel IB-F sheets, 25 mm × 75 mm, plastic backing) to allow increased separation distance. In these cases, the solvent front took ~20 min to travel 70 mm (i.e. 55 mm separation distance).

Samples of [^{177}Lu]Lu-PSMA-617 were spotted onto RP-18 silica gel 60 F_{254} sheets (aluminum backing) and developed with a 75:25 (v:v) mixture of MeOH and DI water with 0.1% TFA. After developing, the plates were dried at room temperature.

To estimate radioactivity of deposited samples, measurements of radioactivity to estimate radioactivity concentration of samples were performed with a calibrated dose calibrator (CRC-25PET, Capintec, Florham Park, NJ, USA).

3.2 Analysis of TLC plates by Cerenkov luminescence imaging

After drying, the plates were imaged for 5 min with a previously-described home-built setup [32], with minor modifications to support radio-TLC plates instead of microfluidic chips. Briefly, the radio-TLC plate was carefully placed on a clearly marked platform within a light-tight chamber, covered with a transparent substrate (i.e., glass microscope slide), and the Cerenkov light (emitted when particles travel sufficiently fast through the glass that they exceed the speed of light in glass) was detected by a scientific cooled camera (QSI 540, Quantum Scientific Imaging, Poplarville, MS) equipped with a 50 mm F/1.2 lens (Nikkor, Nikon, Tokyo, Japan). Some experiments were performed using a thin, transparent plastic scintillator plate instead of glass to increase the light output. After use, glass substrates were discarded and scintillator plates were carefully cleaned, to avoid cross-contamination.

The temperature of the camera was maintained at −10°C for dark current reduction. The field of view was 50 × 50 mm^2.

The raw image comprised an array of values (analog-to-digital units; ADUs) corresponding to detected light at each pixel location. Using custom-written MATLAB software, images were first processed with three corrections as previously described[32], including CCD dark current and bias level correction, lens vignetting and CCD pixel nonuniformity correction, and 3 × 3 median filtering. In addition, we performed background subtraction by selecting an area of the image not containing radioactive sample, computing the average pixel value, and subtracting this average from the pixel values across the whole image. Regions of interest (ROIs) were manually drawn on this final corrected image to enclose the radioactive regions/spots. Each ROI was integrated, and then the fraction of the integrated signal in that ROI (divided by the sum of integrated signal in all ROIs) was computed.

3.3 Analysis of TLC plates via radio-TLC scanner

TLC plates were scanned with a miniGITA TLC scanner (Elysia-Raytest; Straubenhardt, Germany) for 3 min, and the resulting chromatograms were analyzed by GINA-STAR software (Elysia-Raytest). Specifically, the software allowed identification of peaks and integrating the area under the curve (AUC) for each peak. The fraction of total AUC contained within each peak was then computed.

Prior to radio-TLC scanner analysis, TLC plates containing multiple samples of radiopharmaceuticals were first cut into individual “lanes”, each lane corresponding to a single separated sample.

3.4 Comparison of readout with CLI versus a radio-TLC scanner

To assess the accuracy and precision of readout using the CLI method, five TLC plates were spotted with different patterns of activity. (Details of samples and TLC plate preparation are included in the Supplemental Information, Section 7.) Cerenkov images and radio-TLC scans of these plates were obtained as described above. To compare readout methods (CLI and miniGITA scanner), a survey was made that requested participants (experienced operators of radio-TLC scanners; n=8) to analyze the CLI images and the chromatograms obtained with the miniGITA scanner. As a normalization factor, and to account for possible errors in preparing stock solutions and pipetting, the activity in the spots was also measured with an automatic well-type gamma counter (WIZARD 3" 1480, Perkin Elmer, Waltham, MA, USA), after cutting the TLC plates into segments to isolate the individual spots.

4 Results and Discussion

4.1 High-throughput radio-TLC analysis

Recently we have developed droplet-based platforms to perform multiple radiochemical reactions simultaneously that can be used for exploration of reaction parameters and/or to increase the number of replicates of each reaction. Such studies require a means for high-throughput sample analysis. A previously-described home-built Cerenkov imaging setup[32] with minor modifications to support radio-TLC plates instead of microfluidic chips (Figure 1) was used to image the radio-TLC plates. The field of view was 50 mm × 50 mm. When using 5 min acquisitions, the corresponding limit of detection (LOD) and limit of quantification (LOQ) were determined to be 0.8 kBq/μL and 2.4 kBq/μL, respectively, for 1 μL spots of fluoride-18 (Figure S2,S3), and the linear range extended up to 21.3 MBq (Figure S5). The LOD could be further reduced by replacing the glass cover with a scintillator (Figure S4). Even though the sensitivity of our CLI-based scanner (with glass cover) is lower than existing commercial gamma-based radio-TLC scanners (typically reported as ~10 Bq, though the measurement conditions are often unclear), the sensitivity is nevertheless sufficient for analysis of 1 μL spots as we have demonstrated. When needed, the sensitivity can be boosted via the use of scintillator substrate instead of a glass substrate or via improvements in geometry (e.g. using a short lens-to-sample distance).

As an initial demonstration of high-throughput analysis, replicates of both [^{18}F]fallypride (Supplemental Information Section 6) and [^{18}F]FET samples were studied. Two replicates of a sample of the crude intermediate product (collected after fluorination of the FET precursor) were spotted on the left half of the plate and two replicates of a sample of the crude [^{18}F]FET product (collected after the subsequent hydrolysis step) were spotted on the right side. The CL image of the developed TLC plate (35 mm separation distance; silica gel 60 F_{254}) is shown in Figure 2A. At the same time, each sample was also spotted on an additional, longer TLC plate (55 mm separation distance; silica gel IB-F), developed, and scanned with the radio-TLC scanner (sample chromatograms in Figures 2B and 2C). The greater separation resolution of CLI was readily apparent: a low-abundance side product (6 ± 0% of activity, n=2) was easily visible in the CL images (showing 3 distinct regions for both samples), but was not clearly discernable or quantifiable using the radio-TLC scanner software (showing only 2 peaks for each sample). For the pair of samples of the fluorinated

intermediate, percentages of [^{18}F]fluoride, impurity and intermediate determined from the CL image were 27 ± 0 % (n=2), 4 ± 0 % (n=2) and 68 ± 0 % (n=2), respectively. Using the miniGITA scanner after cutting the TLC plate into individual “lanes”, the percentages of [^{18}F]fluoride and intermediate for one “lane” were 32% and 68%, respectively. For the pair of samples of the crude [^{18}F]FET product, percentages of [^{18}F]fluoride, [^{18}F]FET and impurity from the CL image were 15 ± 0 % (n=2), 79 ± 0 % (n=2) and 6 ± 0 % (n=2), respectively. In the analysis from the miniGITA scanner, the percentages of [^{18}F]fluoride and [^{18}F]FET were 19% and 81%, respectively. Aside from the cleaner separation and better resolution, the CLI-based method also had the benefit of faster analysis. The total imaging time for the whole plate (5 min) is independent of the number of samples, while additional scanning time is needed for each strip cut from the radio-TLC plate (4 × 3 min = 12 min).

4.2 Increasing sample throughput

To further increase the number of samples that can be analyzed simultaneously, one option would be to redesign the optical system (including lens) to achieve a larger field of view. Then, a TLC plate (wider than 50 mm) with more spots (“lanes”) could be developed and imaged without increasing the overall analysis time (i.e. without increasing the developing time or readout time). Such an approach would result in a reduction in the number of pixels per imaged spot, however, potentially increasing the noise level slightly and decreasing sensitivity. Additionally, any change in light collection efficiency of the overall system (e.g. moving the camera farther away from the TLC plate) will also affect the signal and the sensitivity.

Alternatively, the size of the radio-TLC plates could be further reduced to allow multiple plates to fit within the field of view. Due to the excellent separation in the Cerenkov images, we hypothesized that the separation length could be even further reduced. Figure 3A shows the separation of 4 crude samples of [^{18}F]Fallypride, with a separation distance of only 15 mm. The radio-TLC plate (silica gel 60 F_{254}) cut to 50 mm × 35 mm size was spotted with two 1 μL droplets and two 0.5 μL droplets at 1 cm spacing along the long edge of the plate, 15 mm from this edge. After developing, the resulting CLI images showed clear separation of the spots, allowing accurate quantification. The fluorination efficiency obtained with the CLI-based analysis for 1 μL spot size was 76 ± 0 % (n=2), and for 0.5 μL spot size was 74 ± 1 % (n=2). To compare with the radio-TLC scanner, each TLC plate was cut into four lanes. The resulting chromatograms showed 78% conversion for 1 μL spot size and 74% for 0.5 μL spot size, but, notably, the peaks exhibited very significant overlap (Figure 3B), which we show, below, can introduce significant errors and uncertainties into the analysis. To further increase the throughput, 8 samples from a batch of crude [^{18}F]Fallypride were spotted (0.5 μL droplet size) on the TLC plate at 5 mm spacing and separated for 15 mm as well (Figure 3C). The fluorination efficiency obtained with the CLI-based analysis appears to be consistent (73 ± 1 %, n=8). In another experiment, 2 different batches (n=4 replicates each batch) of crude [^{18}F]fallypride were analyzed, enabling fluorination efficiency to be easily determined for each (Figure 3D). In addition to being able to fit a larger number of samples in the CLI system field of view, the plate could be developed more quickly (i.e. 2.5 min for the 15 mm separation distance vs. 8 min for 35 mm separation). Though not demonstrated

here, readout throughput could be further increased by placing 2 of these TLC plates within the field of view of the CLI system.

Though it is still practical to manually delineate the multiple ROIs for each of the 8 samples, the analysis process could be further streamlined by developing software tools for automated or semi-automated region segmentation.

4.3 Comparison of readout via CLI versus a radio-TLC scanner

Using five TLC plates spotted with different patterns of activity (2 or 3 separate spots with varying amounts of radioactivity), we obtained a TLC-scan and a CL image, and then asked experienced TLC operators (n=8) to analyze the two sets of data. These data were then normalized using gamma counter measurements of the actual activity in each of the spots on the TLC plate. Results for each of the five sample TLC plates are summarized in Figure 4, and in the Supplementary Information, Table S1.

For all plates, the CLI images showed well-separated spots and participants could readily draw ROIs that accurately contained the activity of each spot. In contrast, the radio-TLC scanner, not equipped with a collimator, showed wide peaks that overlapped in many of the plates. In all cases, the CLI-based results were in better agreement with gamma counter values (lower relative error, i.e. closer to 1.0 value in Figure 4) compared to the radio-TLC scanner based results. This was especially the case when analyzing radio-TLC plates containing regions of unequal radioactivity (i.e. sample plates B, C, and D). Because overlapping peaks are often observed in radio-TLC samples in our laboratory and in the literature, it is likely that many studies contain non trivial quantitation errors. Such errors could be minimized by switching to a CLI-based readout method, or alternatively by improving the radio-TLC method (e.g. installing better collimator, or increasing length of TLC separation).

4.4 Assessing quality of the TLC spotting and development process

One notable advantage of the Cerenkov imaging readout technique versus radio-TLC scanner readout is the ability to see a high-resolution 2D image of the final separation. This can be used to monitor the quality of the spotting and developing process. For example, compared to a normal separation (Figure 5A), we have been able to observe problems such as the splitting of single spots into multiple regions due to incomplete drying of the sample before developing (Figure 5B), poor separation as a result of large spot size (Figure 5C), and non-linear separation path due to accidentally introducing an additional source (droplet) of liquid at the side of the radio-TLC plate during developing (Figure 5D). It should also be possible to detect problems such as double-spotting, or inadvertent contamination of the plate during spotting or subsequent handling. This feedback provides increased information to ensure accurate readout of a given radio-TLC plate or to determine when a TLC (sample spotting and separation) should be re-run.

While not implemented in this study, the CLI readout can be improved by using the same camera to take a bright-field image of the radio-TLC plate (including markings on the TLC plate of sample origin and solvent front) and superimposing the CL image. For example, in the work of Ha *et al.*[31], such superposition allowed confirmation of the multiple positions

where samples were spotted on each TLC plate. An example using our setup, showing both the sample origin and solvent front from the brightfield image (e.g. to compute R_f values), is shown in the Supplemental Information, Section 9.

4.5 Radiochemical purity measurement of [^{177}Lu]-PSMA-617 via CLI

To explore the application of CLI-based radio-TLC analysis to additional isotopes, labeling yield of [^{177}Lu]Lu-PSMA-617 was measured as a function of reaction time by sampling 2 μL crude product (925 kBq/μL) at different time points and spotting on a TLC plate (silica gel 60 RP-18 F_{254}, aluminum backing). The results of CLI analysis in Figure 6 suggest that high labeling efficiency (99%) can be achieved in just 10 min, rather than the typical 30 min timeframe used[1].

5 Conclusion

Cerenkov imaging in combination with parallel developing of multiple samples on a single TLC plate proved to be a practical method for rapid, high-throughput radio-TLC analysis. Compared with a conventional radio-TLC scanner, the CLI-based imaging method provided significantly higher resolution, the ability to image multiple samples in parallel (rather than requiring sequential scanning), and the ability to detect and quantify low-abundance impurities that were not discernable with radio-TLC scanning. The bulk of time and effort savings were realized by spotting multiple samples onto a single TLC plate and developing the multiple samples in parallel prior to imaging, rather than spotting the developing separate TLC plates individually. Furthermore, by leveraging the high resolution of CLI, a much smaller separation distance could be used while still resolving each region of radioactivity, further reducing the time needed for developing the samples. The shorter separation distance in turn can facilitate increased throughput by enabling more TLC plates to be imaged within the field of view; alternatively, the optical system could be redesigned to increase the field of view, thus allowing more spots to be imaged without increasing the system cost.

Quantitative accuracy of the CLI-based readout was found to be higher compared to analysis via the radio-TLC scanner software, and relative uncertainty was lower. This was especially true when chromatograms contained overlapping peaks and/or small peaks. Furthermore, CLI-based analysis enabled detection of quality issues in the spotting or development processes.

TLC in many cases has not historically been considered a reliable test for radiochemical purity and radiochemical identity, mainly due to the lack of appropriate spatial resolution to separate impurities with structural similarities to the product, and lack of quantification opportunity for the product mass and impurity mass. For these reasons, sole reliance on radio-TLC during quality control testing usually can only be established for well-validated manufacturing processes, where a lack of impurities has been previously shown for a high number of runs using cross-validation with an HPLC system, and where the product mass (i.e. molar activity) is not a crucial release control. For example, most GMP sites rely solely on radio-TLC for analysis of [^{18}F]FDG in the routine production for purity by gamma chromatogram readout and identity by comparing retention factor with a cold reference

standard, whereas mass evaluations are performed in periodic quality indicator tests only. As another example, radio-TLC is often used in analysis of radiometal-labeled species, where there is often only one impurity (the unreacted radiometal) and the label and labeled product do not share high chemical similarity. With the introduction of CLI, an inexpensive and high-resolution TLC analysis method has become available. This greatly facilitates the validation of a TLC-based quality control for a new manufacturing process through the much higher sensitivity for impurities.

CLI imaging of TLC plates has broad application for the analysis of radiotracers labeled with radionuclides that are positron emitters (F-18, Cu-64, Zr-89, I-124) used for PET imaging [5,33] and radiopharmaceuticals labeled with beta emitters (e.g., I-131, Lu-177) [34–36]. Though we demonstrated the analysis of ^{18}F-labeled compounds and ^{177}Lu-labeled peptide, this approach could also be used for the analysis of radiopharmaceuticals labeled with alpha emitters (e.g. Ac-225, Bi-213), with applications in targeted radiotherapeutics[37,38]. Previous reports have shown detectable Cerenkov emission from such radionuclides[38,39], likely due to emissions from daughter isotopes [37]. In addition to high-throughput analysis applications, the rapid separation and readout of radio-TLC plates by the method described here could be especially useful in conjunction with very short-lived isotopes such as C-11 (half-life 20.4 min).

Supplementary Material

Refer to Web version on PubMed Central for supplementary material.

Acknowledgments

We thank the UCLA Biomedical Cyclotron Facility for generously providing [^{18}F]fluoride for these studies. This work was supported in part by the National Cancer Institute (R21 CA212718), the National Institute of Mental Health (R44 MH 097271), and the National Institute of Biomedical Imaging and Bioengineering (T32 EB002101). The authors thank Supin Chen, Alex Dooraghi and Prof. Chang-Jin “CJ” Kim for help with early proof-of-concept experiments.

9 References

[1]. Fendler WP, Stuparu AD, Evans-Axelsson S, Lückerath K, Wei L, Kim W, et al. Establishing 177Lu-PSMA-617 Radioligand Therapy in a Syngeneic Model of Murine Prostate Cancer. J Nucl Med 2017;58:1786–92. 10.2967/jnumed.117.193359. [PubMed: 28546332]

[2]. Zacharias P, Gather MC, Rojahn M, Nuyken O, Meerholz K. New Crosslinkable Hole Conductors for Blue-Phosphorescent Organic Light-Emitting Diodes. Angew Chem Int Ed n.d;46:4388–92. 10.1002/anie.200605055.

[3]. Momiyama N, Torii H, Saito S, Yamamoto H. O-nitroso aldol synthesis: Catalytic enantioselective route to α-aminooxy carbonyl compounds via enamine intermediate. Proc Natl Acad Sci 2004;101:5374–8. 10.1073/pnas.0307785101. [PubMed: 15067138]

[4]. Skipski VP, Peterson RF, Barclay M. Quantitative analysis of phospholipids by thin-layer chromatography. Biochem J 1964;90:374–8. [PubMed: 4284220]

[5]. Wang J, Chao PH, Hanet S, Dam RM van. Performing multi-step chemical reactions in microlitersized droplets by leveraging a simple passive transport mechanism. Lab Chip 2017;17:4342–55. 10.1039/C7LC01009E. [PubMed: 29164208]

[6]. Waldmann CM, Gomez A, Marchis P, Bailey ST, Momcilovic M, Jones AE, et al. An Automated Multidose Synthesis of the Potentiometric PET Probe 4-[18F]Fluorobenzyl-

Triphenylphosphonium ([18F]FBnTP). Mol Imaging Biol 2018;20:205–12. 10.1007/s11307-017-1119-1. [PubMed: 28905308]

[7]. Brom M, Franssen GM, Joosten L, Gotthardt M, Boerman OC. The effect of purification of Ga-68-labeled exendin on in vivo distribution. EJNMMI Res 2016;6:65 10.1186/s13550-016-0221-8. [PubMed: 27518873]

[8]. Leonard JP, Nowotnik DP, Neirinckx RD. Technetium-99m-d, 1-HM-PAO: a new radiopharmaceutical for imaging regional brain perfusion using SPECT--a comparison with iodine-123 HIPDM. J Nucl Med Off Publ Soc Nucl Med 1986;27:1819–23.

[9]. Madru R, Kjellman P, Olsson F, Wingårdh K, Ingvar C, Ståhlberg F, et al. 99mTc-labeled superparamagnetic iron oxide nanoparticles for multimodality SPECT/MRI of sentinel lymph nodes. J Nucl Med Off Publ Soc Nucl Med 2012;53:459–63. 10.2967/jnumed.111.092437.

[10]. Price EW, Zeglis BM, Cawthray JF, Lewis JS, Adam MJ, Orvig C. What a Difference a Carbon Makes: H4octapa vs H4C3octapa, Ligands for In-111 and Lu-177 Radiochemistry. Inorg Chem 2014;53:10412–31. 10.1021/ic501466z. [PubMed: 25192223]

[11]. Asti M, Tegoni M, Farioli D, Iori M, Guidotti C, Cutler CS, et al. Influence of cations on the complexation yield of DOTATATE with yttrium and lutetium: a perspective study for enhancing the 90Y and 177Lu labeling conditions. Nucl Med Biol 2012;39:509–17. 10.1016/j.nucmedbio.2011.10.015. [PubMed: 22172388]

[12]. Ha NS, Sadeghi S, van Dam RM. Recent Progress toward Microfluidic Quality Control Testing of Radiopharmaceuticals. Micromachines 2017;8:337 10.3390/mi8110337.

[13]. Ory D, Van den Brande J, de Groot T, Serdons K, Bex M, Declercq L, et al. Retention of [18F]fluoride on reversed phase HPLC columns. J Pharm Biomed Anal 2015;111:209–14. 10.1016/j.jpba.2015.04.009. [PubMed: 25898315]

[14]. Sherma J, DeGrandchamp D. Review of Advances in Planar Radiochromatography. J Liq Chromatogr Relat Technol 2015;38:381–9. 10.1080/10826076.2014.941265.

[15]. Decristoforo C, Zaknun J, Kohler B, Oberladstaetter M, Riccabona G. The use of electronic autoradiography in radiopharmacy. Nucl Med Biol 1997;24:361–5. 10.1016/S0969-8051(97)00055-3. [PubMed: 9257336]

[16]. Jeon SJ, Kim KM, Lim I, Song K, Kim JG. Pixelated scintillator-based compact radio thin layer chromatography scanner for radiopharmaceuticals quality control. J Instrum 2017;12:T11003 10.1088/1748-0221/12/11/T11003.

[17]. Othman N, Talib Y, Kamal WHBW. Imaging Scanner Usage in Radiochemical Purity Test. Nucl Tech Conv 2011.

[18]. Gillies JM, Prenant C, Chimon GN, Smethurst GJ, Perrie W, Hamblett I, et al. Microfluidic reactor for the radiosynthesis of PET radiotracers. Appl Radiat Isot 2006;64:325–32. 10.1016/j.apradiso.2005.08.007. [PubMed: 16290944]

[19]. Fujibayashi Y, Cutler C, Anderson C, McCarthy D, Jones L, Sharp T, et al. Comparative studies of Cu-64-ATSM and C-11-Acetate in an acute myocardial infarction model: ex vivo imaging of hypoxia in rats. Nucl Med Biol 1999;26:117–21. 10.1016/S0969-8051(98)00049-3. [PubMed: 10096511]

[20]. von Guggenberg E, Penz B, Kemmler G, Virgolini I, Decristoforo C. Comparison of different methods for radiochemical purity testing of [99mTc-EDDA-HYNIC-D-Phe1,Tyr3]-Octreotide. Appl Radiat Isot 2006;64:194–200. 10.1016/j.apradiso.2005.07.019. [PubMed: 16139504]

[21]. Savolainen H, Windhorst AD, Elsinga PH, Cantore M, Colabufo NA, Willemsen AT, et al. Evaluation of [18F]MC225 as a PET radiotracer for measuring P-glycoprotein function at the blood–brain barrier in rats: Kinetics, metabolism, and selectivity. J Cereb Blood Flow Metab 2017;37:1286–98. 10.1177/0271678X16654493. [PubMed: 27354093]

[22]. Maneuski D, Giacomelli F, Lemaire C, Pimlott S, Plenevaux A, Owens J, et al. On the use of positron counting for radio-Assay in nuclear pharmaceutical production. Appl Radiat Isot 2017;125:9–14. 10.1016/j.apradiso.2017.03.021. [PubMed: 28390998]

[23]. Cho JS, Taschereau R, Olma S, Liu K, Chen Y-C, Shen CK-F, et al. Cerenkov radiation imaging as a method for quantitative measurements of beta particles in a microfluidic chip. Phys Med Biol 2009;54:6757–71. [PubMed: 19847018]

[24]. Cho JS, Douraghy A, Olma S, Liu K, Chen YC, Shen CK, et al. Čerenkov radiation imaging as a method for quantitative measurements of beta particles in a microfluidic chip. Proc. IEEE Nucl. Sci. Symp. NSS Conf, 2008, p. 4510–5.

[25]. Mitchell GS, Gill RK, Boucher DL, Li C, Cherry SR. In vivo Cerenkov luminescence imaging: a new tool for molecular imaging. Philos Trans R Soc Math Phys Eng Sci 2011;369:4605–19. 10.1098/rsta.2011.0271.

[26]. Spinelli AE, D'Ambrosio D, Calderan L, Marengo M, Sbarbati A, Boschi F. Cerenkov radiation allows in vivo optical imaging of positron emitting radiotracers. Phys Med Biol 2010;55:483 10.1088/0031-9155/55/2/010. [PubMed: 20023328]

[27]. Holland JP, Normand G, Ruggiero A, Lewis JS, Grimm J. Intraoperative Imaging of Positron Emission Tomographic Radiotracers Using Cerenkov Luminescence Emissions. Mol Imaging 2011;10:72902010.00047. 10.2310/7290.2010.00047.

[28]. Liu H, Carpenter CM, Jiang H, Pratx G, Sun C, Buchin MP, et al. Intraoperative Imaging of Tumors Using Cerenkov Luminescence Endoscopy: A Feasibility Experimental Study. J Nucl Med Off Publ Soc Nucl Med 2012;53:1579–84. 10.2967/jnumed.111.098541.

[29]. Park JC, An GI, Park S-I, Oh J, Kim HJ, Ha YS, et al. Luminescence imaging using radionuclides: a potential application in molecular imaging. Nucl Med Biol 2011;38:321–9. 10.1016/j.nucmedbio.2010.09.003. [PubMed: 21492780]

[30]. Spinelli AE, Gigliotti CR, Boschi F. Unified approach for bioluminescence, Cerenkov, β, X and γ rays imaging. Biomed Opt Express 2015;6:2168–80. 10.1364/BOE.6.002168. [PubMed: 26114036]

[31]. Ha YS, Lee W, Jung J-M, Soni N, Pandya DN, An GI, et al. Visualization and quantification of radiochemical purity by Cerenkov luminescence imaging. Anal Chem 2018;90:8927–35. 10.1021/acs.analchem.8b01098. [PubMed: 29991252]

[32]. Dooraghi AA, Keng PY, Chen S, Javed MR, Kim C-J CJ Chatziioannou AF, et al. Optimization of microfluidic PET tracer synthesis with Cerenkov imaging. Analyst 2013;138:5654–64. 10.1039/C3AN01113E. [PubMed: 23928799]

[33]. Knowles SM, Tavare R, Zettlitz KA, Rochefort MM, Salazar F, Jiang ZK, et al. Applications of immunoPET: using 124I-anti-PSCA A11 minibody for imaging disease progression and response to therapy in mouse xenograft models of prostate cancer. Clin Cancer Res 2014:clincanres.1452.2014 10.1158/1078-0432.CCR-14-1452.

[34]. Baum RP, Kulkarni HR, Schuchardt C, Singh A, Wirtz M, Wiessalla S, et al. 177Lu-Labeled Prostate-Specific Membrane Antigen Radioligand Therapy of Metastatic Castration-Resistant Prostate Cancer: Safety and Efficacy. J Nucl Med 2016;57:1006–13. 10.2967/jnumed.115.168443. [PubMed: 26795286]

[35]. Chatalic KLS, Konijnenberg M, Nonnekens J, de Blois E, Hoeben S, de Ridder C, et al. In Vivo Stabilization of a Gastrin-Releasing Peptide Receptor Antagonist Enhances PET Imaging and Radionuclide Therapy of Prostate Cancer in Preclinical Studies. Theranostics 2016;6:104–17. 10.7150/thno.13580. [PubMed: 26722377]

[36]. Kraeber-Bodéré F, Rousseau C, Bodet-Milin C, Ferrer L, Faivre-Chauvet A, Campion L, et al. Targeting, Toxicity, and Efficacy of 2-Step, Pretargeted Radioimmunotherapy Using a Chimeric Bispecific Antibody and 131I-Labeled Bivalent Hapten in a Phase I Optimization Clinical Trial. J Nucl Med 2006;47:247–55. [PubMed: 16455630]

[37]. Kratochwil C, Bruchertseifer F, Giesel FL, Weis M, Verburg FA, Mottaghy F, et al. 225Ac-PSMA-617 for PSMA-Targeted α-Radiation Therapy of Metastatic Castration-Resistant Prostate Cancer. J Nucl Med 2016;57:1941–4. 10.2967/jnumed.116.178673. [PubMed: 27390158]

[38]. Ruggiero A, Holland JP, Lewis JS, Grimm J. Cerenkov luminescence imaging of medical isotopes. J Nucl Med Off Publ Soc Nucl Med 2010;51:1123–30. 10.2967/jnumed.110.076521.

[39]. Pandya DN, Hantgan R, Budzevich MM, Kock ND, Morse DL, Batista I, et al. Preliminary Therapy Evaluation of 225Ac-DOTA-c(RGDyK) Demonstrates that Cerenkov Radiation Derived from 225Ac Daughter Decay Can Be Detected by Optical Imaging for In Vivo Tumor Visualization. Theranostics 2016;6:698–709. 10.7150/thno.14338. [PubMed: 27022417]

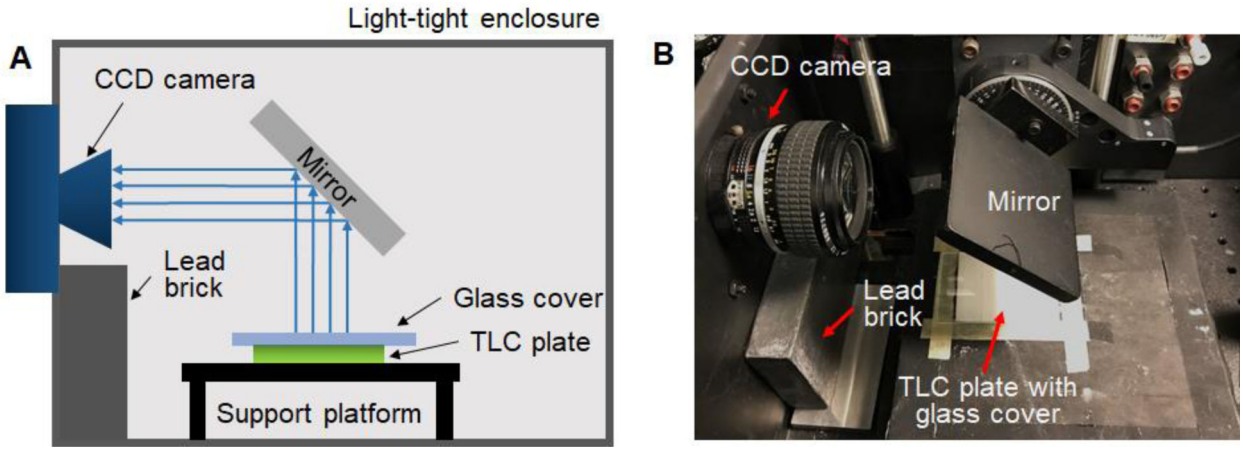

Figure 1.

Cerenkov luminescence imaging setup within the light-tight enclosure. (A) Schematic. (B) Photograph.

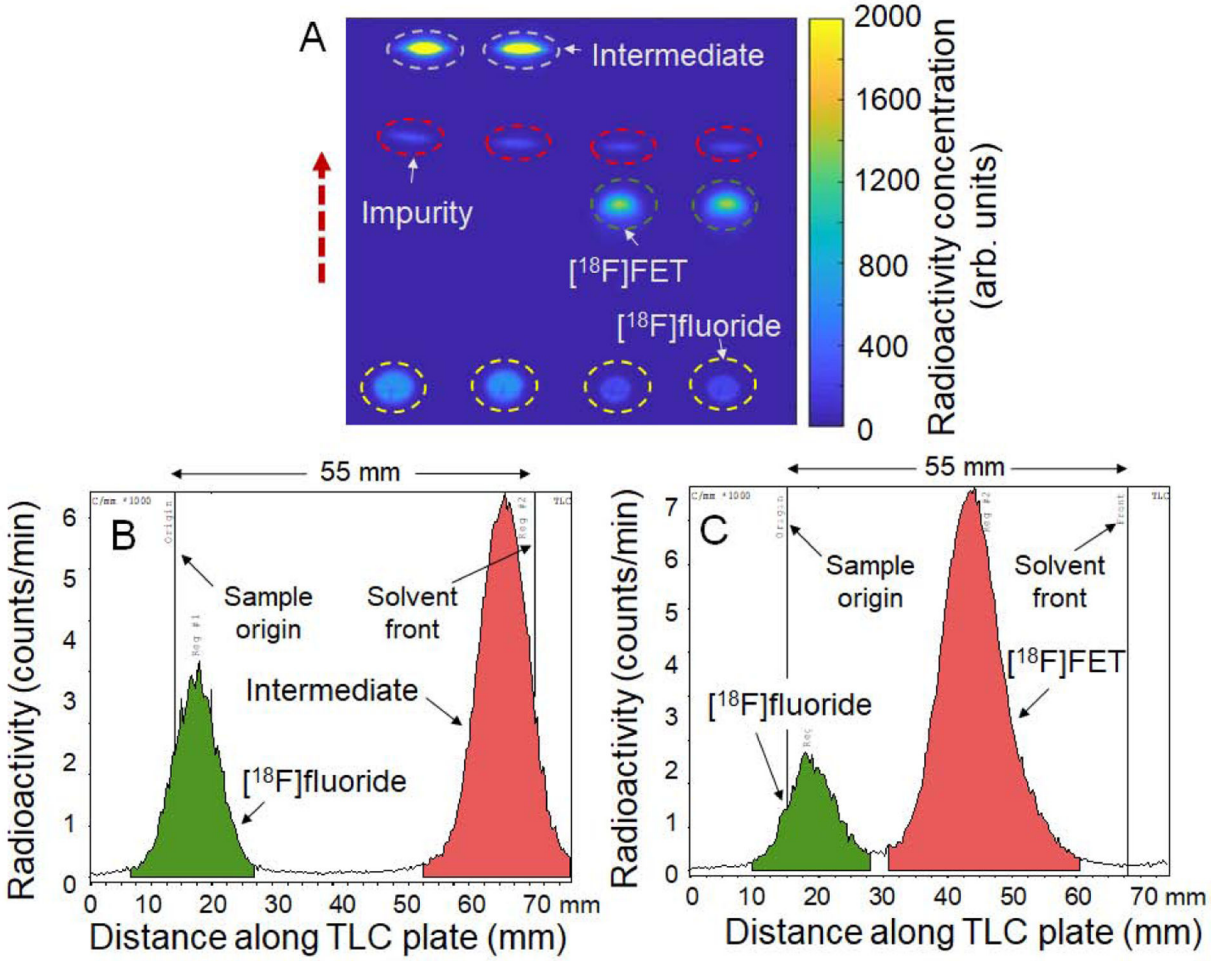

Figure 2.

High-throughput analysis of [^{18}F]FET samples. (A) Cerenkov image of developed TLC plate spotted with two replicates of crude fluorination product (1 μL each) and two replicates of crude hydrolysis product (1 μL each). The dashed circles indicate the ROIs used for analysis. The dashed arrow indicates the direction of solvent movement during developing. (B) Example chromatogram obtained with the radio-TLC scanner spotted with crude fluorination product. (C) Example chromatogram from radio-TLC scan of crude hydrolysis product. Note that for B and C, the samples were spotted onto a different TLC plate and separation performed over 55 mm instead of 35 mm (in the Cerenkov image) to try to enhance separation between the species, but the low-abundance impurity could not be discerned.

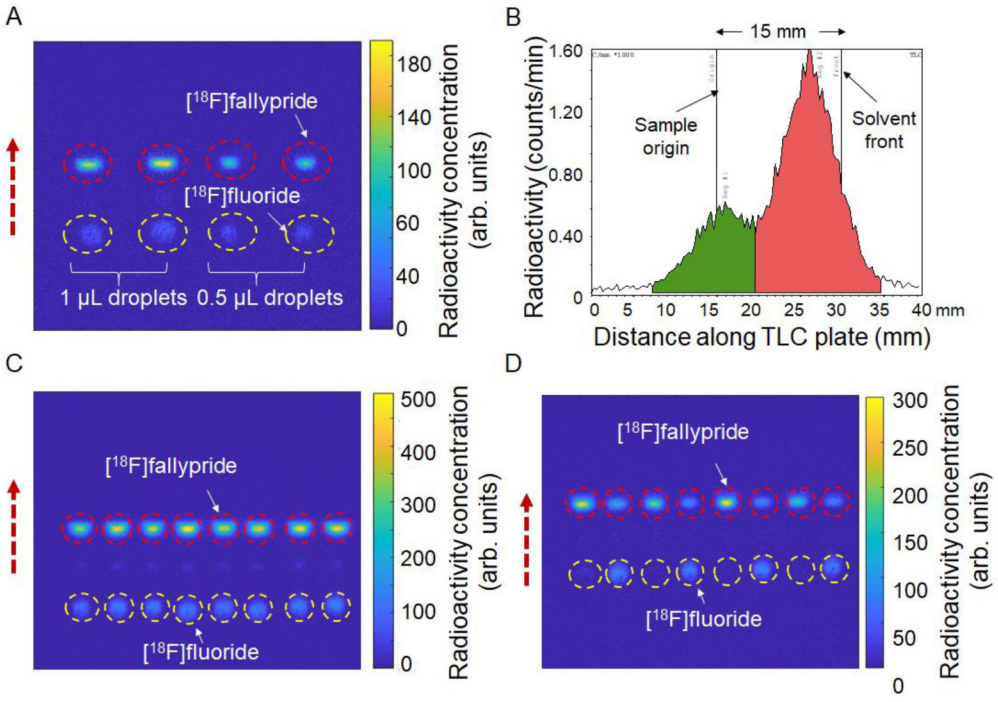

Figure 3.

High-throughput analysis of crude [^{18}F]fallypride samples. (A) Cerenkov image of developed TLC plate spotted with 4 replicates (two 1.0 μL and two 0.5 μL) of the same crude reaction mixture using only 15 mm separation distance. (B) One example chromatogram obtained from the 0.5 μL sample in (A) using the radio-TLC scanner. The TLC plate was first imaged with the CLI based scanner and then was cut into 4 “lanes” each of which was scanned separately with miniGITA scanner. (C) Cerenkov image of developed TLC plate spotted with 8 replicates (0.5 μL) of another batch of crude [^{18}F]fallypride. The dashed circles represent the ROIs for analysis. The dashed arrow represents the direction of solvent flow during developing. (D) Cerenkov image of developed TLC plate spotted with 8 droplets (0.5 μL) sampled from 8 different batches of crude [^{18}F]fallypride reacted under different sets of conditions (n=4 replicates each of two different sets of conditions, spotted in alternating pattern).The dashed circles highlight the ROIs for the 8 samples. The dashed arrow represents the direction of solvent flow during developing.

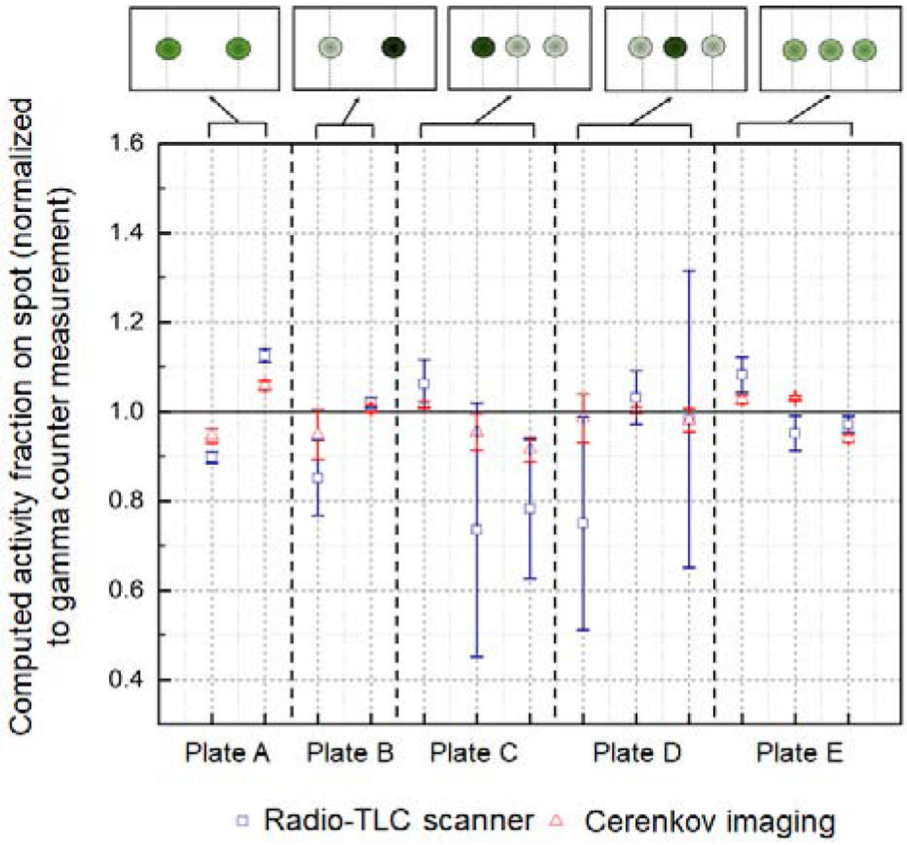

Figure 4.

Radio-TLC readout performance comparison of radio-TLC scanner (blue squares) and Cerenkov luminescence (red triangles) of the plates in Figure S8. The data points show the average activity fraction in each spot (averaged over the analysis performed by n=8 participants) normalized by the activity fraction determined by gamma counting. The normalized activity fraction provides a measure of accuracy. Values close to 1.0 indicate high accuracy, i.e., close agreement between the result from the radio-TLC scanner or Cerenkov luminescence analysis and the gamma counter measurement of the radioactivity in a particular spot. The error bars show the relative standard deviations and indicate the precision. The black dashed vertical lines separate the data from each of the five radio-TLC plates. Cartoons of the activity distribution are shown at the top of the graph (darker green spots represent higher activity level).

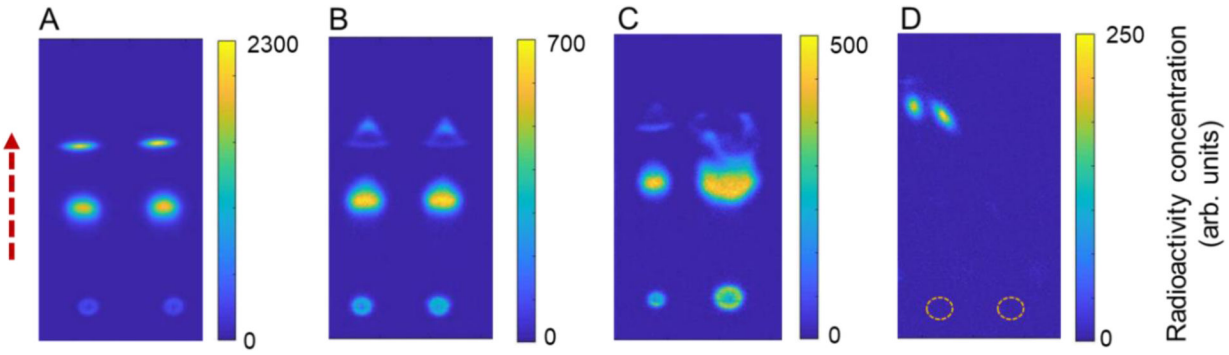

Figure 5.

Assessing quality of the TLC spotting and developing process. (A) Cerenkov image of developed plate after spotting of two replicates (1 μL) each of crude [^{18}F]FET product. This image indicates a normal spotting and developing process. (B) Separation artifacts visible in most distant spots when the plate was not completely dried prior to developing. (C) Separation artifacts due to a combination of incomplete drying as well as abnormally large sample volume (right spot 2.0 μL). (D) Separation artifacts arising from liquid contamination at the right edge of the TLC plate during developing, causing the main solvent flow to be deflected to the left. The TLC plate in this case was spotted, at the positions marked with dash circles, with two replicates (1 μL each) of crude [^{18}F]fallypride product.

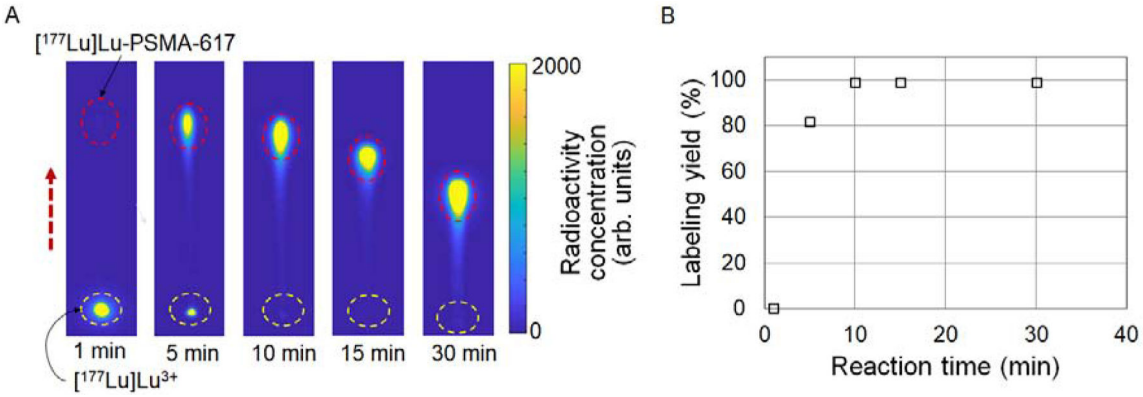

Figure 6.

CLI-based analysis of crude [^{177}Lu]Lu-PSMA-617 samples (β^--emitter). (A) Cerenkov image of developed TLC plates spotted with droplets (2 μL) of the crude reaction mixture sampled at different reaction times. In this demonstration, each TLC plate was developed individually, resulting in variable separation distances, but multiple plates were imaged together. The dashed circles represent the ROIs for analysis. The dashed arrow represents the direction of solvent flow during developing. (B) Graph of radiolabeling yields as a function of reaction time.